NEW MATERIALS AND APPLICATIONS FOR MAGNETIC TUNNEL JUNCTIONS

G. REISS, J. SCHMALHORST, H. BRÜCKL, A. THOMAS, J. SCHOTTER,
M. BRZESKA, A. HÜTTEN, AND S. KÄMMERER

Department of Physics, University of Bielefeld, P.O. Box 100 131, 33501 Bielefeld, Germany

Abstract: In magnetolectronic devices large opportunities are opened by the spin dependent tunnelling resistance, where a strong dependence of the tunnelling current on an external magnetic field can be found. Within a short time, the quality of the junctions increased dramatically. We will address first the issue of new materials with large spin polarization as ferromagnetic electrodes; using Co_2MnSi, TMR values up to 100% can be achieved at low temperature. The properties of these junctions are, however, not yet at optimum. Possible reasons will be discussed and improvements suggested. Next, the influence of the geometry of small tunnelling junctions especially on the magnetic switching behaviour is considered down to junction sizes below $0.01\,\mu m^2$. The last part will give a short overview on applications beyond the use of the tunnelling elements as storage cells in MRAMs. This concerns mainly field programmable logic circuits, where we demonstrate the clocked operation of a programmed AND gate. The second 'unconventional' feature is the use as sensing elements in DNA or protein biochips, where molecules marked magnetically with commercial beads can be detected *via* the dipole stray field in a highly sensitive and relatively simple way.

1. INTRODUCTION

Magnetic tunnelling junctions (MTJs) [1, 2] are one of the currently most investigated systems with respect to their magnetic and magnetotransport properties. This is due to the growing interest in the basics of spin dependent transport and spin injection as well as due to their potential for applications in electronic devices [3, 4]. One major interest is to find new materials as ferromagnetic electrodes which produce larger effects than the traditional $3d$ ferromagnets and their alloys (although their limits concerning the TMR effect are not yet clear). One of the class of materials of interest in this context are ferromagnetic Heusler alloys, which are predicted to be ferromagnetic half metals, meaning that there is a gap at the Fermi level for only one spin direction of the conduction electrons. This in consequence leads to "100% spin-polarization P", *i.e.* at the Fermi level only states for one spin direction are available [5].

In this work we first present results for a Heusler alloy integrated into MTJs. As example, we chose Co_2SiMn. As full Heusler alloy, this is one of the materials with possibly large spin polarization [5]. First examples show, that this material can be successfully integrated into MTJs as ferromagnetic electrode giving up to 100% resistance change at low bias voltage and temperature; the value of the room temperature TMR, however, is still below the numbers obtained with conventional ferromagnets. Reasons for that will be discussed and possible improvements suggested.

The next decisive property of the MTJs is their scalability, meaning that for a successful integration into electronic devices they should show no deterioration of the tunnelling magnetoresistance down to about 200 nm for nowadays devices and down to 50 nm for being applicable for a reasonable number of years. Thus, in the next section atomic and magnetic force microscopy (MFM) try to give insight in the complex magnetic properties of individual MTJs [6-8]. The geometry of the MTJs and the roughness on the nanometer scale can disturb the magnetic switching behaviour; we show, however, that shapes can be found which give rise to a reproducible single domain like switching behaviour. On MTJs smaller than 200 nm, the limited MFM resolution hinders imaging; thus, we employed conducting force microscopy [9] for taking complete asteroids on MTJs as small as 50 nm which turn out to maintain the TMR amplitude even down to this size.

The paper will close with the discussion of applications beyond MRAM's, *e.g.*, field programmable logic circuits [10] and the use as sensing elements in DNA or protein biochips [11, 12].

2. NEW MATERIALS

First attempts to form reliable MTJ's tried to use one relatively hard and one relatively soft ferromagnetic electrode. This, even if the hard electrode is additionally stabilized by an antiferromagnetically coupled trilayer, turned out to be not particularly stable, because the domain splitting of the soft electrode causes large stray fields which induce a deterioration of the hard magnetic material [13, 14]. Moreover, often Cu was found to diffuse to the interface with the barrier and to destroy quickly the TMR effect.

The minor loops therefore were not suitable for storing one bit due to the obvious instabilities produced by the interaction of the soft with the hard magnetic electrode. Within a short time, however, major breakthroughs concerning the demands on magnetic stability could be obtained by the combination of antiferromagnetic materials (*e.g.* PtMn, IrMn) with antiferromagnetically coupled trilayers like CoFe/Ru/CoFe, which are much more stable than Co/Cu/Co both magnetically as well as concerning diffusion properties. Using such layer systems, TMR values between up to 70% combined with reproducible switching behaviour can now been obtained [15].

Larger effect amplitudes, however, would still be of major importance especially concerning the development of programmable logic devices. Moreover, for the vision of a complete family of magnetoelectronic devices, a switch with very large resistance ratio between on and off state is of central importance.

Heusler alloys with a predicted gap at the Fermi level for one spin direction are very promising candidates for further increasing the TMR amplitude. We thus prepared thin films of the (so called full) Heusler alloy Co_2SiMn with a predicted magnetic moment of $5\mu_B$ per formula unit and a gap of around 0.4 eV [5], both critically depending on the degree of ordering.

The MTJs are prepared at room temperature by DC- and RF-magnetron sputtering on thermally oxidized Si(100) wafers with a typical growth rate of 0.3 nm/s. For investigating the $Co_2MnSiAlOx$ interface by surface sensitive XAS, two different half MTJs are grown:

Stack A: $V^{42\,nm}$ / $Co_2MnSi^{d(CMS)}$ with d(CMS) = 4, 8, 15, 61 and 100 nm / $Al^{1.4\,nm}$ + plasma oxidation for 200 s + *in-situ* annealing at about 450°C for 1 h.

Stack B: $V^{42\,nm}$ / $Co_2MnSi^{100\,nm}$ / $Al^{1.4\,nm}$ without intentional oxidation (the thickness of the individual layer is given as superfix; note, that the Vanadium serves as seed layer in order to promote a textured growth of the Co_2MnSi [16]).

For investigating the transport properties of full MTJs, a 5 nm thick $Co_{70}Fe_{30}$ layer, magnetically hardened and exchange-biased by a subsequent antiferromagnetic $Mn_{83}Ir_{17}$ (10 nm) layer, is additionally deposited on the type A (d(CMS) = 100 nm) half junction. For these samples, the upper electrode is deposited after the *in-situ* annealing step without breaking the vacuum. Finally, the full MTJs are covered by an upper conduction layer and subsequently patterned by optical lithography and ion beam etching (quadratic junction area 10000-90000 μm^2). The full MTJs are vacuum annealed for 1 h at 275°C in a magnetic field of 1 kOe to set the exchange bias of the upper $Co_{70}Fe_{30}$ electrode.

Figure 1 shows results of a magnetization measurement of this complete stack and the tunnelling characteristic (I / V curve).
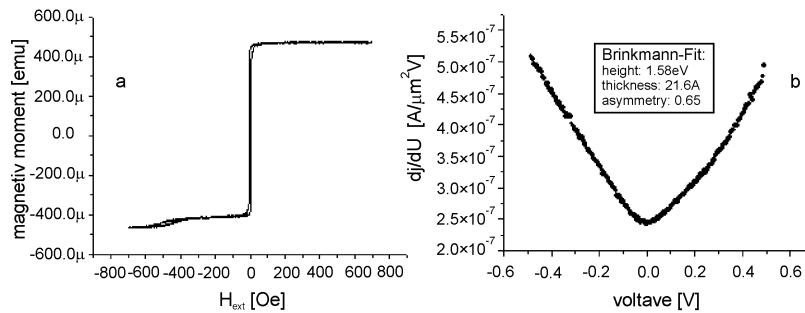
Fig. 1. a) Magnetic moment as a function of an external magnetic field (major loop) for the MTJ described in the text. b) The corresponding I/V curve of the MTJ with the results from the Brinkmann-fit

The magnetization shows a very well separated switching of the thin pinned (small step in Fig. 1a) and the thicker Heusler-electrode, which is a necessary precondition for observing meaningful TMR values. Moreover, we obtain at room temperature a magnetic moment of about 4.5 μ_B per formula unit [16] close to the predicted value at 0 K. The current voltage characteristic, however, is not yet at optimum. Evaluating the I/V curve of Fig. 1b [17], gives a minimal area resistance product R_{min} = 13.3 G$\Omega\mu m^2$ of the Heusler containing MTJ which is about 400 times higher than that of a standard MTJ with NiFe electrode (MTJ-NiFe), although the Al thickness prior to oxidation is identical (1.4 nm) and the oxidation conditions are comparable. At room temperature a typical MTJ-NiFe is characterized by a mean barrier height of 2.89 ± 0.10 eV and a barrier thickness of 1.76 ± 0.09 nm. Therefore, the increase of the barrier thickness of only 0.5 nm for the MTJ-CMS (Fig. 1b) can account for its higher

resistance because of the exponential dependence of the area resistance product on the barrier thickness for direct tunneling.

Additionally, a barrier height of only 1.6 eV and a large barrier asymmetry of 0.6 eV are not typical for "good" tunnelling barriers of Al_2O_3. Although the I/V curve therefore is not in an optimum for obtaining large TMR values, the tunnelling elements with Heusler alloy electrode do produce a reasonably large TMR value of around 33% at room temperature and of up to 100% at 10 K, critically depending on the bias voltage (see Fig. 2).
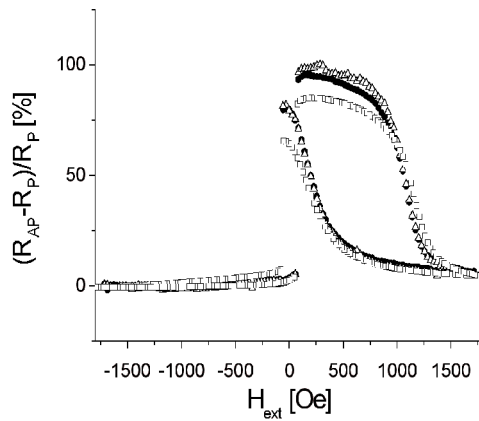
Fig. 2. The TMR for a tunnelling junction including the Heusler alloy Co_2SiMn as soft magnetic electrode at 10 K, 20 K and at room temperature for different bias voltages: $\triangle$: 100×100 μm², 0.5 mV, 20 K: $P_{Co2MnSi} = 67\%$. ■: 200×200 μm², 0.5 mV, 20 K, □: 200×200 μm², 10 mV, 10 K

Especially the low temperature TMR is among the largest as compared to conventional $3d$ ferromagnets. The strong temperature dependence, however, again is unusual for "good" tunnelling junctions, where, *e.g.,* a decrease from about 70% to 50% can be found.

Thus there should be considerable further improvements possible by further work concentrating on the preparation of better interfaces and tunnelling barriers on top of the Heusler alloy. One of the first properties which have to be investigated in this context is the roughness. A large roughness can give rise to a varying thickness of the barrier with local under- and overoxidation and to magnetostatic coupling of the electrodes. Selected samples thus were investigated by AFM (Digital Instruments Nanoprobe IIIa), but the evaluation of the roughness gave typically values around 0.4 nm rms, which is the same as for conventional MTJs.

In order to better understand the non-ideal I/V curve, the relatively strong temperature dependence of the TMR and the details of the interfaces between Heusler alloy and tunnelling barrier, additional XAS measurements in normal incidence were performed [18] at the PEEM-2 beamline 7.3.1.1 at the Advanced Light Source, Berkeley, USA.

For Mn the type B sample with only naturally oxidized Al shows a structureless L2,3-absorption edge shape (Fig. 3), typically for delocalized $3d$ electrons, like in metallic Mn. In contrast, the plasma oxidized samples (type A) have a pronounced multiplett structure (indicated by the arrows in the lower part of Fig. 3), independent from the Co_2MnSi thickness and annealing procedure.

The multiplett structure clearly hints to an increased localization of the $3d$ electrons. The energy positions of the additional peaks agree quite well with calculated XAS spectra assuming a $6S_{5/2}$ ground-state term. Especially, this line shape is found for oxidized Mn. As shown also by Auger depth profiling, a Mn (and possibly also a Si-) segregation to the interface between the Co_2MnSi and the barrier for plasma oxidized samples is observed. The formation of MnO_x is now verified by

Fig. 3. XAS spectra of a type A and a type B sample with d(CMS) = 100 nm. The photon energy is defined with respect to the maximum of the L3-absorption edge. The arrows indicate additional features in the XAS of type A samples in comparison to the type B sample
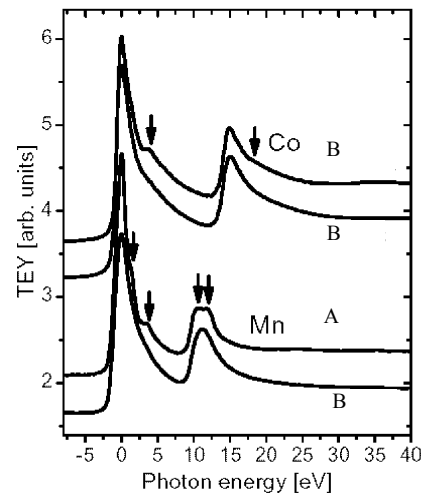
by the development of the Mn-multiplett structure in all plasma oxidized samples. Thus, the presence of oxygen at the interface between barrier and the Co_2MnSi obviously leads to the formation of MnO_x and possibly a diffusion of Mn to the interface region. Up to now, the chemical state of the Si in the interface region could not be investigated by XAS because of experimental restrictions. Usually, the MnO_x multiplett structure for pure oxide films is significantly sharper. In the samples investigated here, however, the measured shape of the Mn-L2,3-edges of the plasma oxidized type A samples results from a superposition of a signal from MnO_x in the interface region and a signal from the underlying (not oxidized) Mn of the Heusler alloy. In contrast to Co, which showed the additional shoulder 4 eV above the resonances, no clearly visible change of the absorption edge shape after annealing is found.

3. JUNCTION SIZE AND SHAPE

The geometrical shape of micro- and nanoscale magnetic patterns is known already for a long time to strongly influence the magnetic behaviour. Thus we investigated this dependence with special regard to the application driven demands put on the MTJs.

Junctions with different shapes and sizes were investigated: rectangular MTJs ranging from 700×700 nm^2 to 700×1400 nm^2 and elliptical patterns with 500 nm short axes and 850 nm long axes. The patterns were covered by a 15 nm thick Ta layer which minimizes stray field effects of the homemade, CoCr covered MFM tip and, hence, tip induced perturbations of the

soft layer's magnetization. Sufficient signal to noise ratio and small perturbations were obtained for a CoCr thickness of 30 nm.

As an example, we discuss a typical result obtained with MFM measurements for elliptical junctions (Fig. 4, [8]). Although they often show a high remanent magnetization, the shape favors vortex formation and the magnetization reversal often needs high saturation fields. In or near saturation the NiFe electrodes show a high magnetic contrast at their end points. At $H = 1$kA/m the magnetization shows four opposite regions with bright or dark contrast, typical for a vortex state (Fig. 4). Thicker films show similar patterns more pronounced due to the larger stray fields. It should be noted, that considerably different magnetic behaviour was found for nominally identical shapes. This could be traced back to the individually shaped edges of the patterns which result from the grainy structure of the films and the e-beam resist. Frequently, domain wall pinning was found at kinks or bumps at the edge as small as around 10 nm.

H = 6 kA/m   H = -1 kA/m   35 nm NiFe

1 μm   phase shift   -0.2 deg   0.2 deg
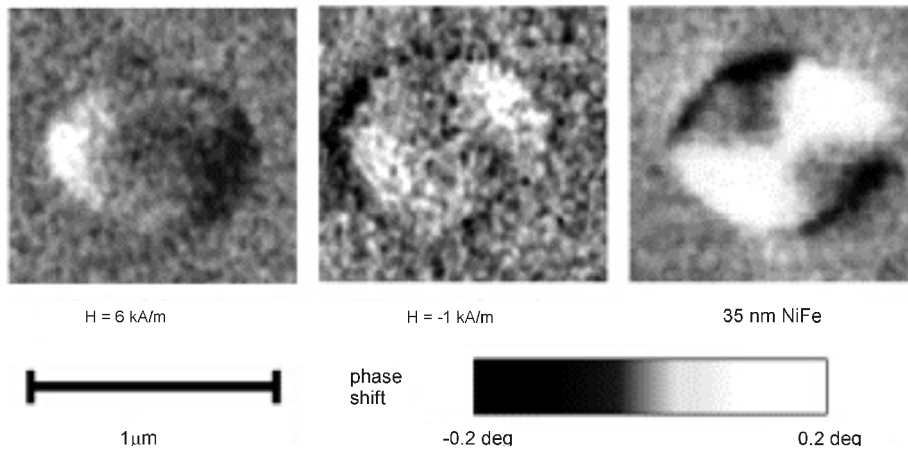
Fig. 4. MFM images of elliptically patterned 5 nm thick $Ni_{80}Fe_{20}$ TMR electrodes recorded at different stages of the minor loop with a vortex in the pattern. Additionally an experimental MFM image of a vortex state in a 35 nm thick NiFe ellipse is shown
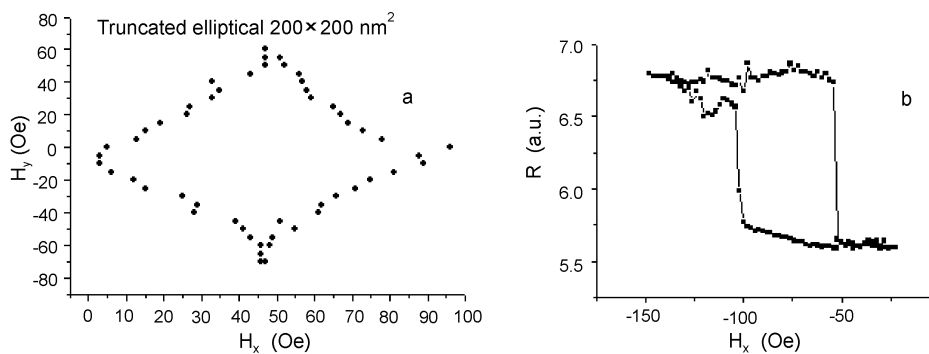
Fig. 5. Astroid of a truncated elliptically shaped MTJ with a reproducible switching behavior (a) and a single minor loop for a circular MTJ with a diameter of 50 nm (b)

MTJs smaller than around 300nm did not produce enough signals for a reliable MFM measurement. We therefore customized a commercial AFM for electrical measurements witha diamond coated conducting tip [9]. With this instrument, we were able to take TMR minor loops of junctions with sizes down to around 50 nm. Whereas on rectangular and elliptical MTJs results similar those of the MFM investigations were obtained, for sizes down to about 100 nm, truncated elliptically shaped patterns turned out to show a reproducible switching behavior as illustrated in Fig. 5a by an astroid for a nominally 200 nm wide MTJ.

On junctions with sizes well below 100 nm we were up to now unable to take complete astroids due to problems resulting from the relatively large tip radii of the diamond coated AFM tips. Thus, in Fig. 5b, only a typical minor loop for a 50 nm circular MTJ is shown. For these ultrasmall elements, we never observed steps in the minor loops or unusually large saturation fields which would point to switching *via* domain states or vortex formation, respectively. This and the shape of the minor loops therefore suggest a single domain behaviour at these small sizes, which could be a considerable advantage regarding downscaling issues.

4. APPLICATIONS BEYOND MRAM

TMR-effects can have considerably broader field of applications than only as storage cells for MRAMs. Processing units from magnetic tunnelling cells could, *e.g.*, considerably contribute to create a complete technology platform based on these junctions. Thus, we concentrate first on the use in field programmable logic gate arrays, which is most closely related to the MRAM development in respect mainly to ASICs and embedded memories in logic chips.

Field programmable logic Gate Arrays from Magnetic Tunnelling Cells

Logic gate arrays are electronic circuits producing an output voltage which is defined as logic function of input signals such as, *e.g.*, "AND" or "NAND". Field programmable means that the logic function of a gate array can be changed during the operation of the processing unit. Up to now, this is done by SRAM and FLASH, where programming is time consuming
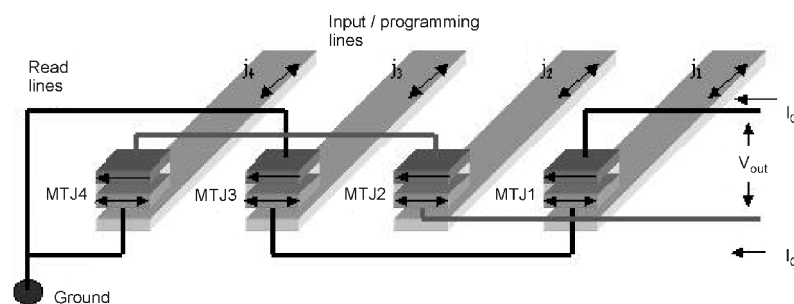
Fig. 6. Bridge configuration of MTJs. The input/programming lines produce a magnetic field that rotates the soft magnetic electrode's magnetization, changing the output voltage V_{out}, which represents the logic function of the inputs

and requires relatively large voltage in an, *e.g.*, floating gate architecture. Using a bridge configuration of TMR cells as shown in Fig. 6 could overcome these drawbacks.

Here, the input is represented by currents on two input lines, which can change the magnetization state of the MTJs soft electrodes. Two neighbouring lines are used to set the resistance states of the other two MTJs which 'programme', *i.e.* define the value V_{out} obtained as logic function of the two inputs.

In Figure 7, we show a clocked operation of such an arrangement with a programmed "AND" function [10]:
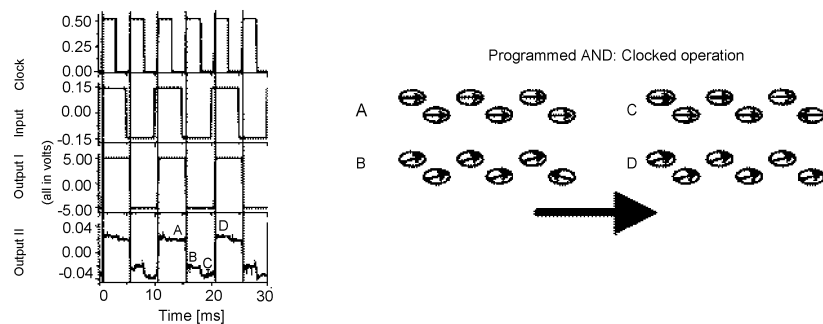
Fig. 7. Clocked operation of six MTJs in a bridge arrangement of sic MTJs. Output I is a rectified signal of the original V_{out} (output II). The right side shows the magnetization states corresponding to the different outputs A to D

This feasibility study thus demonstrates that MTJs can be used in logic gate arrays which are programmable "on the fly". The large advantages of this "Magnetic Logic" are scalability (similar to MRAM), and speed. Programming these arrays will be as fast as the logic operation with typical time scales down to the nsec regime. This opens in turn new perspectives for innovative schemes like reconfigurable computing [19].

Magnetic Biochips

As the last example, we now turn to a completely different field: In biotechnology and medical applications, molecules like DNA or proteins are frequently marked by magnetic spheres called "beads". These beads often consist of magnetite embedded in a polystyrene matrix and are commercially available with sizes down to around 100 nm and an already functionalized shell. Functionalized means in this context, that, *e.g.*, streptavidin molecules are attached to the beads which are able to bind very specifically and tightly to, *e.g.*, biotin molecules which in turn can be specifically attached to DNA or proteins.

This opens the possibility to measure the presence or absence of these biomolecules by detecting the magnetic beads with an MTJ. Baselt *et. al.* [11] already described this technique using Giant Magnetoresistance sensors. Figure 8 shows the principle of this method and the result of the measurement of different bead concentrations with a 100 μm wide TMR cell [12].

As can be seen in Fig. 8, reasonable signals as in dependence of the perpendicular field are obtained at a surface coverage of only a few percent, if an in plane field is additionally applied

which brings the soft electrode close to switching. Comparisons with the established optical method of marking with fluorescent molecules showed, that the magnetic biosensor can be more sensitive at low concentrations of the analyte molecule, which is the most interesting area of application.
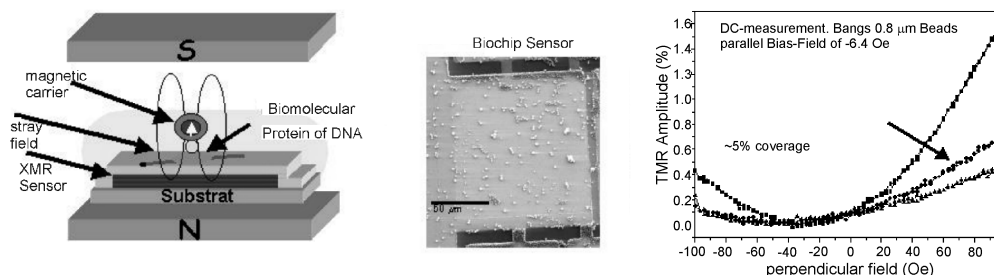
Fig. 8. Principle of the magnetic biochip (left): Biotin marked DNA-molecules hybridize with complementary strands attached to the surface.and streptavidin coated beads then bind to the biotin. By applying a magnetic field perpendicular to the surface, only the in plane components of the dipole stray field of the beads are detected. A TMR sensor surface covered by magnetic beads (middle) and the TMR signal measured during applying a magnetic field perpendicular to the sensor surface and an in plane field which is close to the switching field of the soft electrode (right)

In order to test the ultimate sensitivity and to check out, if even single molecule detection can be possible with the TMR sensor, we again customized an AFM. Here, we use the home-made MFM-tips for imaging a TMR cell and simultaneously detect the resistance change of the MTJ in dependence on the position of the MFM tip on top of the soft electrode. Simultaneously, an in plane field is applied in order to detect the sensor's response to the stray field of the tip in different magnetization states. This stray field does not give rise to domain formation or switching but only rotates the local magnetization by some degrees. This technique on one hand mimics the presence of one bead at the sensor surface and gives on the other hand
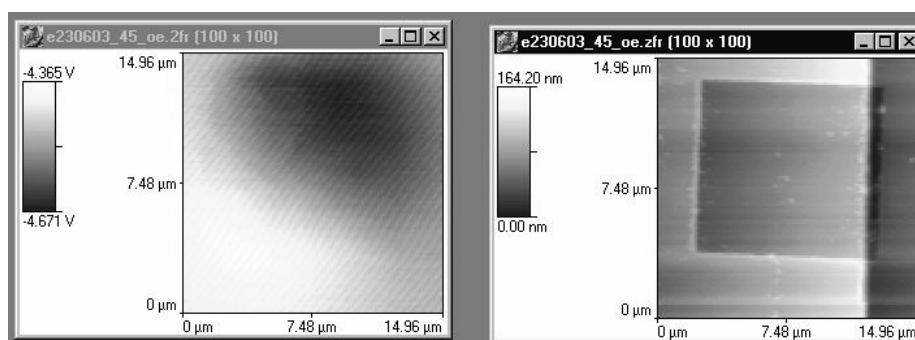
Fig. 9. AFM topography of a 100 μm rectangular TMR cell (right) and the resistance change of the MTJ (left) during imaging with an MFM tip

In this example, we applied an in plane field, which drives the soft (top-) electrode close to switching. As can be seen in Fig. 9, reasonably large signals are produced by the MTJ even

with this relatively large cell size due to the magnetic stray field of the MFM tip, which was covered by 20 nm CoCr. Thus the detection of single beads and thereby of single molecules should be possible with this type of biosensor.

This MFM based characterization technique, however, provides also new information about the TMR cell itself, because the response of the MTJ to a locally concentrated field can be measured in different states of the magnetization process, *i.e.* for different values of the external in plane field. Both experimental work as well as simulations are thus on the way in order to evaluate the potential of this method for a detailed characterization of MTJs especially considering different shapes and edge roughness.

5. CONCLUSIONS

We discussed influences of materials and geometry on the properties of magnetic tunnel junctions. New materials as, *e.g.*, Heusler alloys can be integrated into current standard MTJs, allowing to reliably testing the TMR amplitude. Although the 100% spinpolarization predicted theoretically has not yet been seen in 'real' MTJs, promising results have been obtained and further improvements seem to be straightforward.

For the magnetization switching, effects of edge roughness seem to be a critical point, although certain shapes have been successfully designed for a single domain like switching. At sizes below 100 nm, no signs of domain splitting or vortex formation have been seen up to now, which is very promising for the further downscaling of MTJ storage devices.

Beyond MRAMs or read heads, MTJs can be used for a field programmable magnetic logic, where programming is as fast as the logic operation itself, opening the field of reconfigurable computing and magnetic logic with embedded MRAM memory. Moreover, MTJs are not only able to detect bits on hard disks but also magnetic micro- and nanoparticles which are already in use for biotechnological and medical applications. Proof of principle experiments even demonstrate, that a detection of single molecules should be possible by using MTJs in magnetic biochips. A possible production of MRAMs could thus boost much more possible applications still ahead.

References

[1] J. S. Moodera, L. R. Kinder, T. M. Wong, and R. Meservey, Phys. Rev. Lett. **74**, 3273 (1995).
[2] T. Miyazaki and N. Tezuka, J. Magn. Magn. Mater. **139**, 231 (1995).
[3] S. S. P. Parkin, K. P. Roche, M. G. Samant, P. M. Rice, R. B. Beyers, R. E. Scheuerlein, E. J. O'Sullivan, S. L. Brown, J. Bucchigano, D. W. Abraham, Y. Lu, M. Rooks, P. L. Trouilloud, R. A. Wanner, and W. J. Gallagher, J. Appl. Phys. **85**, 5828 (1999).
[4] G. Reiss, H. Brückl, A. Hütten, J. Schmalhorst, M. Justus, A. Thomas, and S. Heitmann, phys. stat. sol. (b) **236**, 289 (2003).
[5] S. Ishida, T. Masaki, S. Fujii, and S. Asano, Physica B **245**, 1 (1998).
[6] U. K. Klostermann, R. Kinder, G. Bayreuther, M. Rührig, G. Rupp, and J. Wecker, J. Magn. Magn. Mat. **240**, 305 (2002).
[7] Yu Lu, R. A. Altman, A. Marley, S. A. Rishton, and P. L. Trouilloud, Appl. Phys. Lett. **70**, 2610 (1997).
[8] D. Meyners, H. Brückl, and G. Reiss, J. Appl. Phys. **93**, 2676 (2003).
[9] H. Kubota, Y Ando, T. Miyazaki, G. Reiss, H. Brückl, W. Schepper, J. Wecker, and G. Gieres, J. Appl. Phys. **94**, 2028 (2003).
[10] R. Richter, L. Br, J. Wecker, and G. Reiss, Appl. Phys. Lett., **80**, 1291 (2002).
[11] D. R. Baselt, G. U. Lee, M. Natesan, S. W. Metzger, P. E. Sheehan, and R. J. Colton, Biosens. Bioelectron. **13**, 731 (1998).
[12] J. Schotter, P. B. Kamp, A. Becker, A. Phler, D. Brinkmann, W. Schepper, H. Brückl, and G. Reiss, IEEE Trans. Magn. **38**, 3365 (2002).
[13] S. Gider, B.-U. Runge, A. C. Marley and S. S. P. Parkin, Science **281**, 797 (1998).
[14] J. Schmalhorst, H. Brückl, G. Reiss, G. Gieres, M. Vieth, and J. Wecker, J. Appl. Phys. **87**, 5191 (2000).
[15] A. Thomas, H. Brückl, M. D. Sacher, J. Schmalhorst, and G. Reiss, J. Vac. Sci. Technol. B **21**, 2120 (2003).
[16] S. Kämmerer, A. Thomas, A. Hütten, and G. Reiss, Appl. Phys. Lett. **85**, 79 (2004).
[17] H. Brückl, J. Schmalhorst, G. Reiss, G. Gieres, and J. Wecker, Appl. Phys. Lett. **78**, 1113 (2001).
[18] J. Schmalhorst, S. Kämmerer, M. Sacher, G. Reiss, A. Hütten, and A. Scholl, Phys. Rev. B **70**, 0244426 (2004).
[19] W. C. Black, Jr. and B. Das, J. Appl. Phys. **87**, 6674 (2000).
[20] M. Brzeska, M. Justus, J. Schotter, K. Rott, G. Reiss, and H. Brückl, Molec. Phys. Rep. **39**, 32 (2004).